JCI The Journal of Clinical Investigation

JMJD3 regulates CD4 T cell trafficking by targeting actin cytoskeleton regulatory gene *Pdlim4*

Chuntang Fu, … , Helen Y. Wang, Rong-Fu Wang

J Clin Invest. 2019. https://doi.org/10.1172/JCI128293.

Research In-Press Preview Autoimmunity Cell biology Immunology

Graphical abstract

JMJD3 regulates CD4 T cell trafficking by targeting actin cytoskeleton regulatory gene *Pdlim4*

Chuntang Fu[1,2]*, Qingtian Li[2]*, Jia Zou[2]*, Changsheng Xing[2], Mei Luo[2,3], Bingnan Yin[2], Junjun Chu[2], Jiaming Yu[2], Xin Liu [1,2], Helen Y. Wang[2], Rong-Fu Wang[1,2]

[1]Institute of Bioscience and Technology, Texas A&M University Health Science Center, Houston, Texas 77030, USA. [2]Center for Inflammation and Epigenetics, Houston Methodist Research Institute, Houston, Texas 77030, USA. [3]Xiangya Hospital, Central South University, Changsha 410008, China.

* The authors contribute equally to this work

Correspondence should be addressed to: Rong-Fu Wang at Center for Inflammation and Epigenetics, Houston Methodist Research Institute, Houston, TX 77030, USA. Phone: 713-441-7359. Email: rwang3@houstonmethodist.org

Keywords: H3K27, JMJD3, migration, PDLIM4, T cells

Abstract

Histone H3K27 demethylase, JMJD3 plays a critical role in gene expression and T-cell differentiation. However, the role and mechanisms of JMJD3 in T cell trafficking remain poorly understood. Here we show that JMJD3 deficiency in $CD4^+$ T cells resulted in an accumulation of T cells in the thymus, and reduction of T cell number in the secondary lymphoid organs. We identified PDLIM4 as a significantly down-regulated target gene in JMJD3-deficient $CD4^+$ T cells by gene profiling and ChIP-seq analyses. We further showed that PDLIM4 functioned as an adaptor protein to interact with S1P1 and filamentous actin (F-actin), thus serving as a key regulator of T cell trafficking. Mechanistically, JMJD3 bound to the promoter and gene body regions of *Pdlim4* gene and regulated its expression by interacting with zinc finger transcription factor KLF2. Our findings have identified *Pdlim4* as a JMJD3 target gene that affects T-cell trafficking by cooperating with S1P1, and provided insights into the molecular mechanisms by which JMJD3 regulates genes involved in T cell trafficking.

Introduction

T-cell development in the thymus is a multistep process. Early thymic progenitor cells (TPCs) differentiate into T-cell receptor (TCR)-expressing $CD4^+CD8^+$ double-positive (DP) thymocytes in the cortex, and then mature into single-positive (SP) $CD4^+$ and $CD8^+$ T cells in the medulla (1-3). It is known that T-cell trafficking from the thymus to the periphery and then migration into the secondary lymphoid and peripheral organs are regulated by the dynamic cytoskeleton. The dynamic remodeling of the actin cytoskeleton is a key component of cell locomotion and membrane trafficking (4). Of note, cellular mobility and transmigration through the endothelium requires F-actin binding genes for complex cytoskeletal rearrangements (5). After negative and positive selection, the immature T cells express transcription factor Kruppel-like factor 2 (KLF2) and its target gene sphingosine-1 phosphate receptor 1 (S1P1 encoded by *S1pr1*), which are required for T-cell egress from the thymus and subsequent migration to secondary lymphoid organs (1, 3, 6-11). After thymic emigration, the trafficking of mature CD4 or CD8 single-positive T cells is a major process to allow and regulate their immunosurveillance commitment. The motility capabilities of T cells are coupled to their ability to detect and eliminate pathogens and cancer cells. Tumor can be divided into 'hot' (inflamed) or 'cold' (noninflamed) according to the presence of T cells. The presence of tumor-infiltrating lymphocytes in tumor microenvironment has been reported to correlate well with positive clinical outcomes (12, 13). Thus, the promotion of tumor specific T-cell infiltration into tumor microenvironment would benefit T cell tumor immunotherapy. On the other hand, the abnormal motility capabilities of T cells are coupled to the development of undesirable responses against self-antigens, which is a key step in autoimmune disease progression and the failure of organ transplantation. Recent results show that S1P1 agonist FTY-720 (Gilenya) arrests T cell trafficking and prevents multiple sclerosis relapses (14). Therefore, T lymphocyte trafficking may be an important target for immunotherapy and autoimmune response. However, the molecular mechanisms responsible for T lymphocyte trafficking are still poorly understood.

The methylation state of histones is dynamically regulated by histone methyltransferases and demethylases (15-19). Of note, while trimethylation of the lysine 4 residue of histone 3 (H3K4me3) is usually associated with activation of gene expression, trimethylation of lysine 27 residue of histone 3 (H3K27me3) is conversely associated with repression of gene expression (15-19). Methylation of H3K4 can be mediated by several histone methyltransferases (20), while demethylation of H3K4me3 is mediated by members of the lysine demethylase (KDM) 2 and KDM5 families of lysine demethylases. Di- and trimethylation of H3K27 (H3K27me2/3) are mediated by the polycomb repressive complex 2 (PRC2), which contains the H3K27 methyltransferase enhancer of zeste homolog 2 (EZH2) protein (18, 21). On the other hand, demethylation of H3K27me2/3 is mediated by two H3K27 demethylases, Ubiquitously transcribed tetratricopeptide repeat, X chromosome (Utx, KDM6A) and Jumonji Domain Containing 3 (JMJD3, KDM6B) (22-26). Genetically modified *Utx*-deficient mice develop severe heart defects during development, leading to embryonic lethality (27). Similarly, *Jmjd3* whole-body-knockout mice die shortly after birth (28, 29). Although JMJD3 has been implicated in the thymic egress (30), its target genes and the regulatory mechanisms in T cell trafficking have not been reported.

Here, we show that T-cell trafficking from the thymus to the spleen and lymph nodes (LNs) was markedly altered in *Jmjd3*-deficient T cells. Furthermore, we have identified a new role for PDLIM4, a cytoskeletal protein (31, 32) in mediating T-cell migration by affecting the F-actin remodeling. We have also delineated mechanisms by which JMJD3 stabilizes transcription factor binding to the *Pdlim4* promoter. Specifically, our results indicate that JMJD3 regulates the expression of cytoskeletal PDLIM4 by stabilizing the KLF2-ASH2L complex, and thus controls T-cell trafficking.

Results

Critical role of JMJD3 in T-cell trafficking from the thymus to spleen and lymph nodes

We previously generated T-cell-specific deletion of *Jmjd3* (*Jmjd3* cKO) mice by crossing *Jmjd3*$^{f/f}$ mice with CD4-Cre mice and found that JMJD3 plays a critical role in T-cell differentiation (28). To further

define the role of JMJD3 in the homeostasis of T-cell populations and trafficking, we performed flow cytometric analysis of T cells isolated from the thymus, spleen, and LNs. While thymic CD4 SP T cells and CD8 SP T cells were dramatically increased, the percentages of $CD4^+$ T cells were markedly decreased (approximately 50%) in both spleens and LNs of *Jmjd3* cKO mice as compared to WT mice **(Figure 1, A** and **B)**. Similarly, CD8 SP T cells were also reduced in *Jmjd3* cKO spleens but not in the LNs **(Figure 1, A** and **B)**. Furthermore, the extent of $CD4^+$ T cells, but not $CD8^+$ T cells, was reduced in the peripheral blood of *Jmjd3* cKO mice **(Figure 1C)**. Taken together, these results suggest that CD4-driven deletion of *Jmjd3* results in marked accumulation of thymic CD4 and CD8 SP T cells, thus reducing their ability to migrate from the thymus to secondary lymphoid organs.

Trafficking of WT and JMJD3-deficient T cells in adoptive transfer models

Next, we sought to determine the intrinsic trafficking properties of WT and *Jmjd3*-deficient T-cells in *Rag2*$^{-/-}\gamma c^{-/-}$ recipient mice, which lack endogenous T cells. Adoptive T-cell transfer of equal numbers of thymic WT and *Jmjd3*-deficient CD4 SP T cells demonstrated reduced number of splenic *Jmjd3*-deficient $CD4^+$ T cells than splenic WT cells **(Figure 2A)**, suggesting defective *Jmjd3*-deficient $CD4^+$ T-cell migration. To further substantiate these findings, we performed adoptive transfer of TCR-specific $CD4^+$ T cells. For this purpose, we crossed TCR 2D2 transgenic mice, harboring myelin oligodendrocyte glycoprotein (MOG) peptide-specific TCRs, with *Jmjd3*$^{f/f}$ mice, with or without CD4-Cre to generate 2D2:*Jmjd3*$^{f/f}$ and 2D2:*Jmjd3*$^{f/f}$:cKO mice. Next, CD4 SP thymocytes were isolated by FACS using antibodies against 2D2 TCR (TCRVα3.2 and TCRVβ11) (**Figure 2B** left up panel). Adoptive transfer of equal numbers of these 2D2 TCR-specific T cells from 2D2:*Jmjd3*$^{f/f}$ (WT) and 2D2:*Jmjd3*-cKO mice into sublethally irradiated C57BL/6 mice demonstrated a lower percentage and a lower absolute number of 2D2:*Jmjd3* cKO $CD4^+$ T cells than 2D2 WT $CD4^+$ T cells in the spleens and LNs **(Figure 2B,** right and left down panels**)**, as assessed by flow cytometry of TCRVα3.2 and CD4 cell surface expression. Taken together, these results suggest that *Jmjd3*-deficient $CD4^+$ T cells reduce ability to migrate to the peripheral lymphoid organs, compared with WT control cells.

Next, we sought to determine if the reduced trafficking ability of Jmjd3-deficient CD4+ T cells has functional consequences for the induction of experimental autoimmune encephalomyelitis (EAE), a T-cell-mediated autoimmune disease of the central nervous system (CNS). WT and Jmjd3 cKO mice were immunized by subcutaneous injection of the antigenic peptide for MOG (MOG35-55) plus complete Freund's adjuvant (CFA), and then injected with pertussis toxin (PTx) to induce EAE (**Supplemental Figure 1A**). WT mice developed EAE disease faster and more severely than Jmjd3 cKO mice, as evidenced by mean clinical scores (**Supplemental Figure 1B**).

To further study the role of JMJD3 in tumor therapy, we performed adoptive transfer of TCR-specific $CD4^+$ T cells. For this purpose, we crossed TRP-1 TCR transgenic mice (obtained from the Jackson Laboratory, 008486), which express TCR specific for the minimal tyrosinase-related protein 1 (TRP-1) epitope, with *Jmjd3*$^{f/f}$ and CD4-Cre mice to generate TRP-1:*Jmjd3*$^{f/f}$ and TRP-1:*Jmjd3*$^{f/f}$:cKO mice. Next, $CD4^+$ T cells were isolated from splenocytes by untouched CD4 isolation kit. Equal numbers of these TRP-1 TCR-specific T cells from TRP-1:*Jmjd3*$^{f/f}$ (WT) and TRP-1:*Jmjd3*-cKO mice were adoptive transferred into B16-bearing mice **(Supplemental Figure 1C).** We observed smaller tumors in the mice with WT $CD4^+$ T cells than the mice with *Jmjd3* cKO cells **(Supplemental Figure 1, D and E)**. We next detected the tumor infiltrating T cells by flow cytometry of TCRVα3.2 and CD4 markers, and demonstrated a lower percentage and absolute numbers of TRP-1:*Jmjd3* cKO $CD4^+$ T cells than WT TRP-1 $CD4^+$ T cells in the tumor **(Supplemental Figure 1F)**. Taken together, these results suggest that *Jmjd3*-deficient $CD4^+$ T cells have an impaired ability to migrate to the tumor microenvironment, as compared with WT controls.

Identification of PDLIM4 as a key regulator of T-cell migration

We next sought to identify JMJD3 target genes that might regulate T-cell migration by performing microarray analysis of thymic CD4 SP T cells isolated from WT and *Jmjd3* cKO mice. Gene expression

profiling revealed that 16 genes were markedly downregulated, while 5 were upregulated in thymic *Jmjd3* cKO CD4 SP T cells compared to WT cells **(Figure 3A** and **Supplemental Table 1)**. Changes in genes involved in cell motility, cell death, and cell proliferation were confirmed by quantitative real-time PCR analysis **(Figure 3B)**. Genes, such as *Amigo2*, *Igfbp4*, and *Lgals1*, were downregulated, while *Slc15a2* and *Gbp1* were upregulated in thymic *Jmjd3* cKO CD4 SP T cells when compared with WT CD4 SP T cells **(Figure 3B)**. We also observed that the expression of *Ccr7* and *Cd62l* were remarkably downregulated in *Jmjd3*-deficient CD4 SP T cells **(Figure 3B)**. However, there was no significant difference in the expression levels of several other genes, such as *Erdr1*, *Samhd1*, *Akr1c18*, and *Adam11,* between WT and *Jmjd3* cKO CD4 SP T cells **(Supplemental Figure 2A)**. *S1p1* and *Pdlim4* (encoding the PDZ and LIM domain protein 4), but not *Klf2*, were significantly downregulated in thymic *Jmjd3* cKO CD4 SP T cells compared to WT CD4 SP T cells **(Figure 3B)**. We further tested their expression at the protein level. The western blotting data showed the dramatic decrease of S1P1 in Jmjd3 cKO cells (**Supplemental Figure 2B**). However, We did not observe an appreciable difference in CCR7 protein between WT and Jmjd3 cKO cells. This observation was further supported by flow cytometry analysis of CCR7 on the surface of WT and *Jmjd3* cKO CD4 SP T cells **(Supplemental Figure 2C)**.

Since PDLIM4 has been identified as a modifier of actin filament dynamics through its interaction with alpha-actinin and F-actin (33), we postulated that PDLIM4 might contribute to the migration defects in *Jmjd3* cKO $CD4^+$ T cells. To test this possibility, we constructed GFP-expressing retroviral vectors containing *Jmjd3* and *Pdlim4*. Splenic T cells were collected from 2D2:*Jmjd3*$^{f/f}$ (WT) and 2D2:*Jmjd3* cKO mice and activated in vitro before transduction with GFP-containing viruses. GFP^+ $CD4^+$ T cells were sorted, and equal numbers of GFP^+ cells were adoptively transferred into irradiated C57BL/6 recipient mice. After 48 h, single-cell suspensions were prepared from the isolated spleens and LNs of the recipient mice. MOG_{35-55} peptide-specific donor cells were analyzed by flow cytometry using 2D2 TCR specific antibodies (TCRVα3.2 and TCRVβ11). Ectopic expression of *Jmjd3* or *Pdlim4*, but not the empty vector control, restored the number of 2D2:*Jmjd3* cKO $CD4^+$ T cells in the spleens and LNs

similar to 2D2:*Jmjd3*$^{f/f}$ (WT) CD4$^+$ cells **(Figure 3C)**, suggesting that *Jmjd3* or *Pdlim4* may rescue any defects in T cell migration.

To further determine whether PDLIM4 could rescue the CD4$^+$ T-cell migration defect due to *Jmjd3* deficiency, we isolated bone marrow cells from either WT or *Jmjd3*-cKO mice and overexpressed control-GPF or *Pdlim4*-GFP in these bone marrow cells **(Figure 3D)**. We generated chimeric mice, in which these bone marrow cells were transplanted into sublethally irradiated C57BL/6 mice. Flow cytometric analysis of splenocytes and thymocytes from these chimeric mice showed that significantly higher percentage of *Jmjd3* cKO CD4$^+$ T cells transduced with control-GFP in thymus but reduced percentage of T cells accumulated in the spleen when compared with WT CD4$^+$ T cells. However, thymic and splenic accumulation of *Jmjd3*-deficient CD4$^+$ T cells was restored upon ectopic expression of *Pdlim4* **(Figure 3D)**.

In order to further demonstrate the physiological role of PDLIM4 in CD4$^+$ T-cell migration, we isolated thymic CD4 SP T cells from WT mice, generated *Pdlim4* knockout CD4$^+$ T-cells using the CRISPR-Cas9 system **(Supplemental Figure 3A)**, labeled the cells with carboxyfluorescein succinimidyl ester (CFSE), and then adoptively transferred them to irradiated C57BL/6 mice. After 48 h, we determined the number of T cells by FACS analysis and found an increased number of *Pdlim4*-knockout CD4$^+$ T cells in the peripheral blood of mice, but reduced number in spleen and LNs, suggesting a decreased ability of these cells to migrate into spleen and LNs **(Figure 3E)**. To further determine whether *Pdlim4* knockout inhibits CD4$^+$ T cell migration, we isolated bone marrow cells from WT mice and knocked out *Pdlim4* using the CRISPR-Cas9 system to generate chimeric mice by transferring *Pdlim4* KO-bone marrow cells into irradiated recipient mice. FACS analysis of cells isolated from these chimeric mice showed higher percentage of *Pdlim4* knockout CD4$^+$ T cells accumulated in the thymus, but reduced percentage of *Pdlim4* knockout CD4$^+$ T cells in the spleen and LNs **(Supplemental Figure 3B)**. Taken together, these results suggest that PDLIM4, the target of JMJD3, plays a critical role in T-cell trafficking.

PDLIM4 regulates T cell migration through interaction with S1P1 and modulation of F-actin organization

PDLIM4 has been identified as a modifier of actin filament dynamics through its interaction with alpha-actinin and F-actin in muscle cells and nonmuscle epithelial cells (33). Furthermore, PDLIM4 cytoskeleton protein contains one PDZ domain, which has been reported to play a key role in anchoring receptor proteins in the membrane to cytoskeletal components (34). Since sphingosine 1-phosphate (S1P) treatment can cause actin cytoskeleton remodeling, we next sought to determine whether S1P treatment regulates PDLIM4-mediated actin remodeling in T cells, which may be required for T cell trafficking. To this end, we isolated WT and *Jmjd3*-deficient CD4 SP thymocytes, treated them with S1P after 12 h starvation with serum free medium, and stained F-actin with Phalloidin after T cells fixation. As shown in Fig. 4A, in the WT and *Jmjd3*-deficient CD4 T cells transfected with *Pdlim4*-GFP, we observed specific localization of PDLIM4 in the lamellipodium structure of F-actin remodeling area. By contrast, we did not observe the specific localization of GFP in lamellipodium structure of F-actin remodeling area in the WT and *Jmjd3*-deficient CD4 T cells transfected with GFP. We next determined whether ectopic expression of PDLIM4 promoted F-actin formation using WT thymic CD4 SP T cells, *Jmjd3* cKO CD4 SP T cells, *Pdlim4* KO CD4 SP T cells and *Pdlim4-expressing Jmjd3* cKO T cells, followed by Phalloidin staining and FACS analysis. We found that F-actin organization was defective in *Pdlim4* KO and *Jmjd3* cKO CD4 SP T cells compared to WT and PDLIM4-expressing cells based on low Phalloidin staining after 30 min of 50 nM S1P treatment (**Figure 4B**). Notably, PDLIM4-expressing cells exhibited the highest Phalloidin staining for F-actin (**Figure 4B**), suggesting that PDLIM4 enhances F-actin formation. To further determine the distribution of insoluble F-actin (pellet) and the soluble G-actin (supernatant), we treated WT and *Jmjd3* cKO CD4 SP T cells with S1P and lysed the treated cells. After removal of cellular debris by low centrifuge at 350 g for 5 min, the supernatants were further centrifuged at 150,000 g for 90 min to separate F-actin (in pellet) from soluble G-actin (in supernatant). The relative distribution of insoluble F-actin (pellet) and the soluble G-actin (supernatant) was analyzed by Western blot. We

found that polymerized F-actin in the *Jmjd3* cKO CD4 SP T cells is dramatically decreased when compared with WT cells (**Figure 4C)**. Collectively, our results suggest that JMJD3 or PDLIM4 deficiency markedly reduces F-actin after S1P treatment, which can be rescued by ectopic expression of PDLIM4.

S1P1 is a G-protein-coupled receptor which binds to the bioactive signaling molecule S1P and activates intracellular signaling pathways that lead to cytoskeleton remodeling and T cell egress from the thymus (35). We next used different immunofluorescences to label PDLIM4, S1P1 and phalloidin to stain F-actin in untreated and S1P treated WT SP CD4 T cells and observed co-localization of PDLIM4 with S1P1 on lamellipodium structure in F-actin remodeling area **(Figure 4D)**. Co-localization of PDLIM4 in S1P1 was quantified by using NIS-Elements Analysis and reached 95% upon S1P stimulation, whereas only 40% of co-localization was observed in the untreated cells (**Supplemental Figure 4A**). Consistently, Co-immunoprecipitation analysis revealed that PDLIM4 was associated with S1P1 in CD4 SP thymocytes **(Figure 4E)**. To determine the specific domains of PDLIM4 involved in the interaction with F-actin, we used purified recombinant GST-PDLIM4 in an in vitro cosedimentation assay to investigate the interaction of PDLIM4 and F-actin. The polymerized actin was incubated with GST-PDLIM4, GST-PDLIM4-N del (PDZ domain deletion) or GST PDLIM4-C del (LIM domain deletion), followed by high-speed centrifuging at 150,000 g for 90 min. The pellets and supernatants were subjected to SDS-PAGE separation after fractionation. We found that GST-PDLIM4 or GST-PDLIM4-N del, but not GST-PDLIM4-C del, were in the pellet fraction (**Figure 4F**), suggesting that the C-terminus of PDLIM4 interacts with F-actin. Since PDLIM4 interacts with S1P1 (**Figure 4E**), we next determined which domain of PDLIM4 was required for interacting with S1P1. We constructed FLAG-tagged Pdlim4-N-del (PDZ domain deletion), C-del (LIM domain deletion), full-length *Pdlim4* and HA-tagged S1P1 and cotransfected into HEK293T cells. Co-immunoprecipitation analysis revealed that the PDZ domain of PDLIM4 was required for interacting with S1P1 (**Figure 4G**). Additionally, we mutated one cysteine amino acid to proline amino acid (C330P) in the c-terminal helix-8 region of S1P1. The Co-IP results

showed that S1P1 could not interact with PDLIM4 containing a mutation in helix-8 region **(Supplemental Figure 4B)**. Based on these findings, we are proposing a model showing that the PDLIM4 interacts with the S1P1 protein at the N-terminal PDZ domain and binds to the actin cytoskeleton through its C-terminal LIM domain (**Figure 4H**).

Expression of *Pdlim4* is co-regulated by JMJD3 and KLF2

During T cell differentiation JMJD3 interacts with key differentiation regulatory transcription factors such as T-bet (28, 36, 37). Hence, we postulated that JMJD3 might also interact with factors involved in T-cell migration, such as KLF2 and S1P1, which are master regulators of T-cell emigration from the thymus (6-11). To test this possibility, we co-transfected 293T cells with FLAG-*Jmjd3* and HA-tagged transcription factor genes, including *Runx2*, *Klf4*, *Klf2*, *Wdr5*, *Fosl1*, *FosB*, *Wnt5a*, and *Nkx2.1* **(Figure 5A)**. Co-immunoprecipitation and immunoblot analysis revealed that JMJD3 interacted with KLF2, FosB, and Nkx2.1 in vitro **(Figure 5A)**. A dual-luciferase assay was performed on 293T cells co-transfected with *Klf2*, *Klf4*, *Runx2*, *Nkx2.1*, *FosB*, *T-bet*, and *Rorc* with or without *Jmjd3* and -1512 bp upstream of mouse *Pdlim4* promoter-linked episomal luciferase vector **(Figure 5B)**. Only KLF2 harbored transcriptional activity in regulating *Pdlim4* expression, and JMJD3 significantly enhanced the ability of KLF2 to induce *Pdlim4* promoter-driven luciferase activity **(Figure 5C)**. JMJD3 did not enhance *Pdlim4* promoter-driven luciferase activity without KLF2, suggesting co-regulation of *Pdlim4* by JMJD3 and KLF2. To determine whether endogenous interactions occur between KLF2 and JMJD3, we collected thymic WT and *Jmjd3*-cKO $CD4^+$ SP T-cell lysates and co-immunoprecipitated with anti-JMJD3 or anti-KLF2 antibodies, and then immunoblotted with anti-KLF2 or anti-JMJD3 antibodies. We observed that KLF2 interacted with JMJD3 in $CD4^+$ T cells **(Figure 5D)**. Next, we dissected the precise *Pdlim4* promoter sequences that were responsible for KLF2 and JMJD3 binding. We constructed a series of *Pdlim4* promoter fragment-linked episomal luciferase vectors and co-transfected 293T cells with KLF2 alone or KLF2 and JMJD3 together **(Figure 5E)**. The dual-luciferase assay indicated that sequences -100 bp upstream of the *Pdlim4* transcriptional start site (TSS) were required for KLF2 binding, and sequences -800 bp upstream of the

Pdlim4 TSS were required for JMJD3 and KLF2 binding **(Figure 5E)** and the luciferase reporter assay using CD4 SP T cells showed consistent results **(Supplemental Figure 5A).** To address whether the interaction between JMJD3 and KLF2 is required for KLF2 binding to the *Pdlim4* promoter, we performed a ChIP-qPCR assay on thymic CD4 SP T cells from WT or *Jmjd3* cKO mice. We found that the binding of KLF2 to the *Pdlim4* promoter was defective in *Jmjd3*-deficient CD4 SP T cells, suggesting that JMJD3 is required for KLF2 binding to the *Pdlim4* promoter **(Supplemental Figure 5B)**. This defective binding of KLF2 to the *Pdlim4* promoter could be rescued by expression of JMJD3 in *Jmjd3* cKO CD4 SP T cells **(Figure 5F)**. Taken together, our results indicate that both JMJD3 and KLF2 are required for binding to the promoter region of *Pdlim4* and both co-regulate the expression of *Pdlim4*.

JMJD3 deficiency alters the methylation state of H3K27 and H3K4 on *Pdlim4* promoter

We previously reported that *Jmjd3* deletion specifically increases H3K27 di- and tri-methylation in $CD4^+$ T cells and also affected H3K4 methylation (28). By dissecting the ChIP-Seq data for individual genes of interest, we found that *Pdlim4* and *S1p1*, but not *Klf2*, were highly bivalently marked in *Jmjd3* cKO CD4 SP T cells **(Figure 6A)**. Both *Klf2* and *S1p1* genes contained high levels of H3K4me3, but little or low levels of H3K27me3. Conversely, the upstream promoter regions of the TSS and even gene body regions of *Pdlim4* harbored high levels of H3K27me3 in *Jmjd3* cKO CD4 SP T cells, which were higher than in WT CD4 SP T cells **(Figure 6A)**. For genes such as *Ccr7*, *Cd62l*, *Cd69*, and *Klf4*, we did not observe appreciable changes in H3K4me3 and H3K27me3 levels **(Supplemental Figure 6)**.

To validate our ChIP-Seq data on the methylation status of *Pdlim4,* we performed ChIP-qPCR using WT CD4 SP T and *Jmjd3*-deficient CD4 SP T cells and antibodies which were used to target H3K4me3 and H3K27me3. Interestingly, we observed a marked decrease in H3K4me3 and a marked increase in H3K27me3 levels on the *Pdlim4* gene promoter in *Jmjd3*-deficient $CD4^+$ T cells as compared with WT cells **(Figure 6B)**, suggesting that downregulation of *Pdlim4* in *Jmjd3* cKO CD4 SP T cells may be a result of changes in these epigenetic markers. To determine whether the demethylase activity of JMJD3 is required for regulating *Pdlim4* expression, a luciferase assay was performed on 293T cells co-

transfected with *Pdlim4* promoter-linked episomal luciferase vector and with *Klf2* in the presence of WT or mutant *Jmjd3* (a loss of demethylase function mutation). WT *Jmjd3* significantly enhanced KLF2-mediated *Pdlim4* promoter activity; whereas mutant JMJD3 failed to enhance KLF2-mediated *Pdlim4* promoter activity **(Figure 6C)**. Altogether, these results suggest that *Pdlim4* gene expression in CD4 SP T cells is dependent on JMJD3-dependent methylation of H3K27/H3K4 on *Pdlim4*, which may regulate T-cell trafficking.

JMJD3 stabilizes the interaction between KLF2-WDR5 and regulates *Pdlim4* expression

JMJD3 also co-regulates H3K4 methylation levels by interacting with the H3K4 methyltransferase complex and transcription factors (28). To determine whether KLF2 also interacts with the H3K4 methyltransferase complex and JMJD3, we performed co-immunoprecipitation and immunoblot analyses on 293T cells co-transfected with HA-*Klf2* and FLAG-tagged *Ash2l, Rbbp5, Wdr5*, and *Dpy30*. KLF2 specifically interacted with WDR5, but not ASH2L, RBBP5, and DPY30 **(Figure 7A)**. To confirm the endogenous interaction of KLF2 with WDR5, we isolated CD4 SP T-cell lysates, co-immunoprecipitated with anti-KLF2 antibody, and immunoblotted with anti-JMJD3, anti-WDR5, and anti-KLF2 antibodies respectively. Our results showed that KLF2 interacted with WDR5 and that JMJD3 was required for stabilizing this interaction **(Figure 7B and Supplemental Figure 5C)**. To dissect the regions responsible for this interaction, we generated HA-tagged N- and C-terminal regions of KLF2 **(Figure 7C)**. 293T cells were co-transfected with HA-*Klf2*, HA-*Klf2-N*, or HA-*Klf2-C* along with either FLAG-*Wdr5* or FLAG-*Jmjd3*. We collected whole cell lysates (WCLs), immunoprecipitated with anti-FLAG beads, and immunoblotted with anti-HA antibody. Our results revealed that the N-terminal region of KLF2 interacts with FLAG-WDR5 and the C-terminal region of KLF2 interacts with FLAG-JMJD3 **(Figure 7, D** and **E)**. To address which regions of JMJD3 are involved in the interaction with either KLF2 or ASH2L, we co-transfected 293T cells with HA-KLF2 and HA-tagged N-terminal, C-terminal, or M-middle regions of *Jmjd3*. WCLs were immunoprecipitated with anti-KLF2 antibody and immunoblotted with anti-HA antibody. We found that the N-terminal region of JMJD3 interacts with KLF2 **(Figure 7F)**. We also

performed co-immunoprecipitation and immunoblot analysis using 293T cells, which were co-transfected with FLAG-ASH2L and HA-N-terminal, C-terminal, and M-middle regions of JMJD3 and found that the C-terminal region of JMJD3 interacts with ASH2L **(Figure 7G)**. Taken together, our results demonstrate that Jmjd3 regulates *Pdlim4* expression by interacting with the transcription factor KLF2 and the H3K4 methyltransferase complex protein ASH2L.

Discussion

During development, early thymic progenitor cells (TPCs) differentiate into T-cell receptor (TCR)-expressing $CD4^+CD8^+$ double-positive (DP) thymocytes in the cortex of thymus, and then mature into single-positive (SP) $CD4^+$ and $CD8^+$ T cells in the medulla (1-3). After negative and positive selection, CD4 SP T cells emigrate from the thymus to the periphery, e.g., peripheral blood, spleen, and LNs. The epigenetic modifier JMJD3 has been shown to play critical role in macrophage and T-cell differentiation, but its role and mechanism in T-cell migration are not clear. In this study, we demonstrate that *Jmjd3* ablation results in diminished emigration of mature CD4 SP T cells from the thymus and decreased numbers of CD4 T cells in secondary lymphoid organs. T-cell migration from the thymus to secondary lymphoid organs is regulated by S1P1, whereas T-cell entry into resting LNs typically requires CD62L and CCR7 (1, 38). It is known that KLF2 regulates expression of *S1p1*, *Cd62l* and *Ccr7* (1). S1P1 is highly expressed in mature SP T cells and mediate SP T cell migration along S1P concentration gradients from the thymus to the periphery. Deficiency in KLF2 or S1P1 leads to impaired thymic egress (3, 8, 39). T cell migration phenotypes in in T-cell-specific *Jmjd3*-deficient mice are similar to KLF2 deficient mice (6), leading to the accumulation of mature SP T cells in the thymus, which is associated with lower numbers of SP T cells in the spleen and LNs, as well as downregulation of *S1p1*, *Cd62l* and *Ccr7*. To further understand how JMJD3 affects T-cell migration, we identified a new JMJD3 target gene, *Pdlim4,* which plays an important role in T-cell trafficking. Although *Pdlim4* is the most downregulated gene, other genes including *S1p1*, *Cd62l* and *Ccr7, but not Klf2,* are also downregulated at the RNA level in

Jmjd3-deficient mature SP T cells. Ectopic expression of *Pdlim4* in *Jmjd3*-deficient $CD4^+$ T cells restores their ability to migrate in both the spleen and LNs. Using chimeric mice and adoptive T-cell transfer experiments, we demonstrated that ablation of *Pdlim4* in $CD4^+$ T cells reduces splenic T-cell accumulation. Furthermore, we showed that removal of H3K27me3 by JMJD3 is a critical event in regulating *Pdlim4 and S1p1* expression, but not in the promoter regions of *Cd62l* and *Ccr7*. Thus, our study identified a previously unrecognized role for PDLIM4 in T-cell migration.

PDLIM4 has been identified as a modifier of actin filament dynamics in muscle cells and nonmuscle epithelial cells (31, 32), but how PDLIM4 regulates T cell migration remains unknown. Our findings present in this study indicate that PDLIM4 overexpression could rescue the F-actin assembly and remodeling deficiency in *Jmjd3*-deficient $CD4^+$ T-cells, thus demonstrating the critical role of PDLIM4 for F-actin organization in thymic CD4 SP T cells. Furthermore, S1P/S1P1 signaling is also known to induced cytoskeleton remodeling by increasing polymerization of actin filaments in T cells (40), but how S1P/S1P1 signaling is linked to cytoskeleton remodeling is not clear. To understand the molecular mechanisms of how PDLIM4 regulates T cell migration, we found that PDLIM4 interacts with S1P1 through the N-terminal PDZ domain and anchors to F-actin through the C-terminal LIM domain. S1P1 has been reported to interact with other proteins through their PDZ domain, such as P-Rex1 (41). However, the triple-serine sequence on the C-terminus of S1P1 does not represent a typical PDZ motif, thus indicating that the interaction between S1P1 and the PDZ domain may require an internal PDZ motif that still locates at intracellular C-terminus of S1P1. Another previous report illustrates that the conserved helix-8 motif in Class-A GPCR is critical for the PDZ domain recognition (42). We found helix-8 motif mutation abolishes the interaction between S1P1 and PDLIM4, suggesting that S1P1 C-terminal helix structure is critical for PDZ domain recognition. Thus, our mechanistic studies suggest that PDLIM4 acts as an adaptor bridging between S1P1 signaling and F-actin remodeling during T cell migration.

Previous studies have shown that due to hypermethylation, significant inhibition of *Pdlim4* expression in prostate cancer is observed (43, 44), but the epigenetic factors responsible for this

hypermethylation at the *Pdlim4* promoter remains to be identified. Consistent with these observations, our ChIP-PCR and ChIP-Seq analyses show a substantial increase in H3K27me3 and a decrease in H3K4me3 in the promoter and gene body regions of *Pdlim4,* as well as *S1pr1* (but to lesser extent) in *Jmjd3*-deficient CD4 SP T cells. However, JMJD3 alone did not enhance *Pdlim4* expression without KLF2, suggesting co-regulation of *Pdlim4* by JMJD3 and KLF2. In contrast, we observed a marked reduction in H3K4me3 (with a small increase in H3K27me3) in the promoter and gene body regions of *S1p1*. Not only does JMJD3 harbor H3K27 demethylase activity, it can also associate with H3K4 methyltransferase complexes and affect H3K4me3 levels at gene promoters. Indeed, we found that JMJD3 directly interacts with ASH2L, a core component of the H3K4 methyltransferase complex (28, 36, 37). We further showed that KLF2 interacts with WDR5, another component of the H3K4 methyltransferase complex. However, JMJD3 is required for stabilizing the interaction between KLF2 with WDR5. Based on these findings, we propose that JMJD3 regulates *Pdlim4* and known KLF2-regulated genes (*S1p1, Cd62l and Ccr7*) by interacting with KLF2, WDR5 and ASH2L in the H3K4 methyltransferase complex. JMJD3 ablation disrupts the KLF2-JMJD3-ASH2L complex, leading to an increase in H3K27me3 and/or a reduction in H3K4me3 in the promoter and gene body of *Pdlim4*, thus down-regulating target gene expression. The changes in H3K4me3 and/or H3K27me3 in the gene body are supported by findings that JMJD3 is involved in the protein complex engaged in transcriptional elongation (45). Thus, our study provides the molecular insights by which JMJD3 regulates *Pdlim4* gene expression through interaction with KLF2, WDR5 and ASH2L as a transcription complex.

In summary, our studies provide genetic evidence that T-cell-specific deletion of *Jmjd3* results in multiple defects in T-cell migration. Gene profiling and ChIP-Seq analysis identifies a JMJD3 target gene *Pdlim4*. Importantly, PDLIM4 bridges S1P1-mediated extracellular signaling and F-actin formation, which is critical for T cell migration and trafficking through its PDZ domain in the N-terminus and LIM domain in the C-terminus. Mechanistically, JMJD3 regulates *Pdlim4* expression through interaction with KLF2, WDR5 and ASH2L in the promoter and gene body regions of *Pdlim4*. Thus, our results have

provided insights into the molecular mechanisms by which JMJD3 and its target PDLIM4 regulate T-cell migration.

Materials and methods

Mice

Jmjd3 $^{f/f}$:CD4-Cre mice were generated as previously described (28). C57BL/6 and 2D2 mice were obtained from The Jackson Laboratory. *Rag2*$^{-/-}\gamma c^{-/-}$ mice were purchased from Taconic. RAG1^{-}B^{w}TRP-1 mice were purchased from the Jackson Laboratory (008684) and crossed with *Jmjd3* $^{f/f}$:CD4-Cre mice. Mouse strains are listed in Supplemental Table 3. All the mice were re-derived using standard embryo transfer and maintained in pathogen-free animal facilities at the Houston Methodist Research Institute. These studies were reviewed and approved by Institutional Animal Care and Use Committee at the Houston Methodist Research Institute.

Preparation of mouse CD4 T cells from thymus and spleen

Thymus and spleen were removed from mice and single-cell suspensions were prepared by mincing and passing through stainless mesh. After removing RBCs by lysis with Tris-NH_4Cl solution, the cells were suspended in RPMI1640 medium with 1% fatty acid-free BSA. The spleen and thymus cells were purified to > 90% of CD4 T cells using a mouse CD4 enrichment kit (ThermoFisher).

Immunoprecipitation and Western blot analysis

For immunoprecipitation, cells were lysed in an ice-cold lysis buffer (40 mM Tris-HCl, pH7.5, 150 mM NaCl, and 1% Triton X-100) with proteinase inhibitor. Supernatants were incubated overnight with primary antibody (2μg) and immunocomplexes were allowed to bind to the protein A/G beads for 90 mins at 4° C. Immunoprecipitates were washed three times with the lysis buffer. Western blotting was performed under conventional conditions after extracting the samples in SDS sample buffer. Protein extracts were separated by SDS-PAGE and electrotransferred onto PVDF membrane (Millipore). The membranes were exposed to primary antibodies, washed, incubated with secondary antibodies and the

proteins were visualized by using Pierce Western Blotting Substrate Plus (Thermo Fisher). All antibody information is listed in Supplemental Table 3.

Flow cytometry

To detect the expression of surface molecules, T cells were first incubated with an anti-Fc receptor Ab (24G2) to reduce nonspecific binding of mAbs, and then they are labeled with the appropriate fluorescent mAbs. Appropriate fluorescein-conjugated isotype-matched, control mAbs were used as negative controls. Cells were analyzed with BD FACS Aria II.

Real-time RT-PCR

Total RNA was extracted from cultured cells with TRIzol (Invitrogen) according to the manufacturer's instructions. Oligo (dT) primers and Superscript III reverse transcriptase (Invitrogen) were used for the generation of cDNA from mRNA. Gene expression was determined by quantitative PCR with SYBR Green MasterMix (ABI), and the reactions were run on an ABIPRISM 7900HT Sequence Detection System (Life Science). Primers used for real-time PCR analysis are shown in Supplemental Table 2. Expression levels are given as the ratio of the target gene to the control gene to correct for variations in the initial amount of mRNA (gene/Gapdh x1000).

Chemotaxis, Phalloidin staining, Immunofluorescence, confocal image analysis

To analyze actin cytoskeleton remodeling induced by S1P and other stimulation, CD4 SP T cells were starved 12 h in RPMI 1640 medium with 1% fatty acid-free BSA at 37°C. Starved T cells were mixed with equal volume matrigel and coated on confocal dish. After 30 minutes at 37°C, the diluted S1P was added to outside matrigel for 3 h at 37°C in 5% CO_2. Cells were washed and fixed with 4% formaldehyde in PBS at room temperature for 20 minutes. Whenever required, cells were first labeled with antibodies against extracellular markers such as CD4, washed, blocked and permeabilized in PBS containing 3%

FBS, and 0.5% Triton X-100 for phalloidin staining, which is specific staining for F-actin. CD4+ T cells in matrigel or poly-lysine coated dish were processed for immunofluorescence as described (33). Slides were imaged using Nikon A1Si confocal imaging system. The image analysis was performed by Image J software.

Bone marrow chimeras

Bone marrow cells were isolated from female C57BL6/J mice (8 to 10 weeks of age). The cells were transfected with either retrovirus vector expressing *Pdlim4* or lentivirus vector containing *Pdlim4* CRISPR/Cas9 genome editing elements. These bone marrow cells were injected into lethally irradiated (950 rads) recipient mice (female C57BL6/J mice of 8 to 10 weeks old).

Retrovirus production and transduction

Jmjd3 and Pdlim4 genes were cloned into retrovirus expression vector with a GFP-expressing cassette (pCLIG-IRES-GFP). Retroviral particles were produced in 293T cells transfected with retroviral vectors plus pCL-ECO retroviral packaging plasmid using Lipofectamine 2000 (Invitrogen). Sorted naïve $CD4^+$ T cells were plated and activated with anti-CD3 and anti-CD28 for 1 day, transduced with retroviral supernatants and were spun at 2500 rpm for 1.5 h at 32°C. After spin infection, the cells were cultured in T cell culture medium and harvested on day 5 for subsequent T-cell transfer experiments.

***Pdlim4* knockout by CRISPR-Cas9 and T cell migration analysis**

Naive thymic CD4 SP T cells collected from Cas9 knock-in mice (Jax 024858) were transduced with lentivirus containing *Pdlim4* sgRNA or control sgRNA plasmids (LentiGuide-puro, Addgene 52963). An equal number of cells (10 million) were labeled by CFSE and intravenously injected into sublethally irradiated C57BL/6 mice and 48 h later peripheral blood was collected from the recipient mice. Single-cell suspensions were prepared from the isolated spleens and LNs of the recipient mice. The CFSE-

labeled CD4 SP T cells isolated from the spleens, LNs, and peripheral blood were analyzed using FACS assay.

F-actin binding assay

F-actin cosedimentation assay was performed as described previously (44) using the Actin Binding Protein Spin Down Assay Kit (Cytoskeleton Inc. BK001) and recombinant GST-PDLIM4 fusion protein. GST-PDLIM4 was mixed with F-actin in F-actin buffer at room temperature for 30 mins and centrifuged at 150,000g for 1.5 hours at 24°C. The supernatants were then removed and the pellets were suspended in the same buffer. Aliquots of pellets and supernatants were mixed with the loading dye and run on a SDS-PAGE gel, followed by Western blot analysis.

Microarray, ChIP-Seq and Chip-PCR analyses

RNA was extracted from three sorted biological replicates of CD4 SP thymocytes from WT and *Jmjd3* cKO mice. Gene expression profiling was conducted using Genomics and Microarray Core Facility of UT Southwestern Medical Center with Illumina whole genome gene expression arrays. Gene transcripts with greater than 1.5-fold difference in expression were analyzed with Ingenuity pathway analysis software. $CD4^+$ T cells from WT and *Jmjd3* cKO mice were purified and a total of 200 ng of DNA was used for the ChIP-Seq library construction. Illumina sequencing was performed according to previously described protocols (46-48). Sequencing reads from H3K4me3 and H3K27me3 ChIP-Seq libraries were aligned to the mouse mm8 genome using ELAND software. In order to reduce PCR amplification bias, only one uniquely mapped read per genomic position was retained. The histone modification changes upon JMJD3 knockout were assessed as follows. The H3K27me3 sequencing reads in WT and cKO samples were counted in 4kb windows centered at TSS or p300 ChIP-Seq peaks. The resulting read counts were used as input to the DEGseq algorithm56 to identify differentially methylated genes and enhancers. The DEGseq q-value cutoff of 0.05 and the fold-change cutoff of 2 were used to identify statistically significant

methylation changes. The GEO (Gene Expression Omnibus) accession number for the raw and analyzed ChIP-seq data is GSE58775. ChIP-PCR experiments were performed using the Imprint Chromatin Immunoprecipitation Kit (Sigma) according to the manufacturer's instructions. Samples in triplicate were used for all experiments. All primers are listed in Supplemental Table 2.

Statistics

Data was analyzed with the GraphPad Prism 4.0 software. Results represent the mean ± SD where applicable. Statistical analyses between two groups were assessed using two-tailed Student's t test. Statistical analyses among three or more groups were assessed by 1-way ANOVA with Tukey's multiple comparisons test. For all tests, a *P* value less than 0.05 was considered statistically significant.

Acknowledgements

We would like to thank Olga A. Guryanova (Lerner Research Institute, Cleveland Clinic, Cleveland, Ohio) for the LCMV-Pdlim4-eGFP plasmids, and Jana S. Burchfield, Joshua C. Korb and Kalpana Mujoo for critical reading and editing of the manuscript. This work was supported by grants from the NCI and NIDA, NIH (R01CA101795 and U54CA210181), Cancer Prevention and Research Institute of Texas (CPRIT; DP150099, RP150611 and RP170537), and Department of Defense (DoD) CDMRP BCRP (BC151081) to R.F.W.

Author Contribution

CF, QL, and JZ contributed equally to this work. The authorship order among co-first authors follows family name alphabetical order. CF, QL, JZ, and RFW conceived and designed the experiments. CF, QL, JZ, ML, CX, BY, JC JY, and XL performed the experiments and developed the reagents. CF, QL, JZ, HYW, and RFW analyzed and interpreted the data. CF, QL, JZ, and RFW wrote the paper.

Conflict of interest

The authors declare that they have no conflict of interest.

References

1. Love PE, and Bhandoola A. Signal integration and crosstalk during thymocyte migration and emigration. *Nat Rev Immunol.* 2011;11(7):469-77.
2. Petrie HT. Cell migration and the control of post-natal T-cell lymphopoiesis in the thymus. *Nat Rev Immunol.* 2003;3(11):859-66.
3. Spiegel S, and Milstien S. The outs and the ins of sphingosine-1-phosphate in immunity. *Nat Rev Immunol.* 2011;11(6):403-15.
4. Lee SH, and Dominguez R. Regulation of actin cytoskeleton dynamics in cells. *Mol Cells.* 2010;29(4):311-25.
5. Samstag Y, Eibert SM, Klemke M, and Wabnitz GH. Actin cytoskeletal dynamics in T lymphocyte activation and migration. *J Leukoc Biol.* 2003;73(1):30-48.
6. Carlson CM, Endrizzi BT, Wu J, Ding X, Weinreich MA, Walsh ER, Wani MA, Lingrel JB, Hogquist KA, and Jameson SC. Kruppel-like factor 2 regulates thymocyte and T-cell migration. *Nature.* 2006;442(7100):299-302.
7. Lee K, Na W, Lee JY, Na J, Cho H, Wu H, Yune TY, Kim WS, and Ju BG. Molecular mechanism of Jmjd3-mediated interleukin-6 gene regulation in endothelial cells underlying spinal cord injury. *J Neurochem.* 2012;122(2):272-82.
8. Matloubian M, Lo CG, Cinamon G, Lesneski MJ, Xu Y, Brinkmann V, Allende ML, Proia RL, and Cyster JG. Lymphocyte egress from thymus and peripheral lymphoid organs is dependent on S1P receptor 1. *Nature.* 2004;427(6972):355-60.
9. Sebzda E, Zou Z, Lee JS, Wang T, and Kahn ML. Transcription factor KLF2 regulates the migration of naive T cells by restricting chemokine receptor expression patterns. *Nat Immunol.* 2008;9(3):292-300.
10. Weinreich MA, Takada K, Skon C, Reiner SL, Jameson SC, and Hogquist KA. KLF2 transcription-factor deficiency in T cells results in unrestrained cytokine production and upregulation of bystander chemokine receptors. *Immunity.* 2009;31(1):122-30.
11. Yamada T, Park CS, Mamonkin M, and Lacorazza HD. Transcription factor ELF4 controls the proliferation and homing of CD8+ T cells via the Kruppel-like factors KLF4 and KLF2. *Nat Immunol.* 2009;10(6):618-26.
12. van der Woude LL, Gorris MAJ, Halilovic A, Figdor CG, and de Vries IJM. Migrating into the Tumor: a Roadmap for T Cells. *Trends Cancer.* 2017;3(11):797-808.
13. Trujillo JA, Sweis RF, Bao R, and Luke JJ. T Cell-Inflamed versus Non-T Cell-Inflamed Tumors: A Conceptual Framework for Cancer Immunotherapy Drug Development and Combination Therapy Selection. *Cancer Immunol Res.* 2018;6(9):990-1000.
14. Garris CS, Wu L, Acharya S, Arac A, Blaho VA, Huang Y, Moon BS, Axtell RC, Ho PP, Steinberg GK, et al. Defective sphingosine 1-phosphate receptor 1 (S1P1) phosphorylation exacerbates TH17-mediated autoimmune neuroinflammation. *Nat Immunol.* 2013;14(11):1166-72.
15. Chi P, Allis CD, and Wang GG. Covalent histone modifications--miswritten, misinterpreted and mis-erased in human cancers. *Nat Rev Cancer.* 2010;10(7):457-69.
16. Cloos PA, Christensen J, Agger K, and Helin K. Erasing the methyl mark: histone demethylases at the center of cellular differentiation and disease. *Genes Dev.* 2008;22(9):1115-40.
17. Klose RJ, and Zhang Y. Regulation of histone methylation by demethylimination and demethylation. *Nat Rev Mol Cell Biol.* 2007;8(4):307-18.
18. Margueron R, and Reinberg D. The Polycomb complex PRC2 and its mark in life. *Nature.* 2011;469(7330):343-9.

19. Mosammaparast N, and Shi Y. Reversal of histone methylation: biochemical and molecular mechanisms of histone demethylases. *Annu Rev Biochem.* 2010;79(155-79.
20. Black JC, Van Rechem C, and Whetstine JR. Histone lysine methylation dynamics: establishment, regulation, and biological impact. *Mol Cell.* 2012;48(4):491-507.
21. Cao R, Wang L, Wang H, Xia L, Erdjument-Bromage H, Tempst P, Jones RS, and Zhang Y. Role of histone H3 lysine 27 methylation in Polycomb-group silencing. *Science.* 2002;298(5595):1039-43.
22. Agger K, Cloos PA, Christensen J, Pasini D, Rose S, Rappsilber J, Issaeva I, Canaani E, Salcini AE, and Helin K. UTX and JMJD3 are histone H3K27 demethylases involved in HOX gene regulation and development. *Nature.* 2007;449(7163):731-4.
23. Hong S, Cho YW, Yu LR, Yu H, Veenstra TD, and Ge K. Identification of JmjC domain-containing UTX and JMJD3 as histone H3 lysine 27 demethylases. *Proc Natl Acad Sci U S A.* 2007;104(47):18439-44.
24. Jepsen K, Solum D, Zhou T, McEvilly RJ, Kim HJ, Glass CK, Hermanson O, and Rosenfeld MG. SMRT-mediated repression of an H3K27 demethylase in progression from neural stem cell to neuron. *Nature.* 2007;450(7168):415-9.
25. Kouzarides T. Chromatin modifications and their function. *Cell.* 2007;128(4):693-705.
26. Lan F, Bayliss PE, Rinn JL, Whetstine JR, Wang JK, Chen S, Iwase S, Alpatov R, Issaeva I, Canaani E, et al. A histone H3 lysine 27 demethylase regulates animal posterior development. *Nature.* 2007;449(7163):689-94.
27. Jin C, Li J, Green CD, Yu X, Tang X, Han D, Xian B, Wang D, Huang X, Cao X, et al. Histone demethylase UTX-1 regulates C. elegans life span by targeting the insulin/IGF-1 signaling pathway. *Cell Metab.* 2011;14(2):161-72.
28. Li Q, Zou J, Wang M, Ding X, Chepelev I, Zhou X, Zhao W, Wei G, Cui J, Zhao K, et al. Critical role of histone demethylase Jmjd3 in the regulation of CD4+ T-cell differentiation. *Nat Commun.* 2014;5(5780.
29. Satoh T, Takeuchi O, Vandenbon A, Yasuda K, Tanaka Y, Kumagai Y, Miyake T, Matsushita K, Okazaki T, Saitoh T, et al. The Jmjd3-Irf4 axis regulates M2 macrophage polarization and host responses against helminth infection. *Nat Immunol.* 2010;11(10):936-44.
30. Manna S, Kim JK, Bauge C, Cam M, Zhao Y, Shetty J, Vacchio MS, Castro E, Tran B, Tessarollo L, et al. Histone H3 Lysine 27 demethylases Jmjd3 and Utx are required for T-cell differentiation. *Nat Commun.* 2015;6(8152.
31. Boumber YA, Kondo Y, Chen X, Shen L, Gharibyan V, Konishi K, Estey E, Kantarjian H, Garcia-Manero G, and Issa JP. RIL, a LIM gene on 5q31, is silenced by methylation in cancer and sensitizes cancer cells to apoptosis. *Cancer Res.* 2007;67(5):1997-2005.
32. Guryanova OA, Drazba JA, Frolova EI, and Chumakov PM. Actin cytoskeleton remodeling by the alternatively spliced isoform of PDLIM4/RIL protein. *J Biol Chem.* 2011;286(30):26849-59.
33. Vallenius T, Scharm B, Vesikansa A, Luukko K, Schafer R, and Makela TP. The PDZ-LIM protein RIL modulates actin stress fiber turnover and enhances the association of alpha-actinin with F-actin. *Exp Cell Res.* 2004;293(1):117-28.
34. Lee HJ, and Zheng JJ. PDZ domains and their binding partners: structure, specificity, and modification. *Cell Commun Signal.* 2010;8(8.
35. Zachariah MA, and Cyster JG. Thymic egress: S1P of 1000. *F1000 Biol Rep.* 2009;1(60.
36. Miller SA, Huang AC, Miazgowicz MM, Brassil MM, and Weinmann AS. Coordinated but physically separable interaction with H3K27-demethylase and H3K4-methyltransferase activities are required for T-box protein-mediated activation of developmental gene expression. *Genes Dev.* 2008;22(21):2980-93.

37. Miller SA, Mohn SE, and Weinmann AS. Jmjd3 and UTX play a demethylase-independent role in chromatin remodeling to regulate T-box family member-dependent gene expression. *Mol Cell.* 2010;40(4):594-605.
38. Masopust D, and Soerens AG. Tissue-Resident T Cells and Other Resident Leukocytes. *Annu Rev Immunol.* 2019.
39. Cyster JG, and Schwab SR. Sphingosine-1-phosphate and lymphocyte egress from lymphoid organs. *Annu Rev Immunol.* 2012;30(69-94.
40. Mudd JC, Murphy P, Manion M, Debernardo R, Hardacre J, Ammori J, Hardy GA, Harding CV, Mahabaleshwar GH, Jain MK, et al. Impaired T-cell responses to sphingosine-1-phosphate in HIV-1 infected lymph nodes. *Blood.* 2013;121(15):2914-22.
41. Li Z, Paik JH, Wang Z, Hla T, and Wu D. Role of guanine nucleotide exchange factor P-Rex-2b in sphingosine 1-phosphate-induced Rac1 activation and cell migration in endothelial cells. *Prostaglandins Other Lipid Mediat.* 2005;76(1-4):95-104.
42. Sensoy O, and Weinstein H. A mechanistic role of Helix 8 in GPCRs: Computational modeling of the dopamine D2 receptor interaction with the GIPC1-PDZ-domain. *Biochim Biophys Acta.* 2015;1848(4):976-83.
43. Vanaja DK, Ballman KV, Morlan BW, Cheville JC, Neumann RM, Lieber MM, Tindall DJ, and Young CY. PDLIM4 repression by hypermethylation as a potential biomarker for prostate cancer. *Clin Cancer Res.* 2006;12(4):1128-36.
44. Vanaja DK, Grossmann ME, Cheville JC, Gazi MH, Gong A, Zhang JS, Ajtai K, Burghardt TP, and Young CY. PDLIM4, an actin binding protein, suppresses prostate cancer cell growth. *Cancer Invest.* 2009;27(3):264-72.
45. Chen S, Ma J, Wu F, Xiong LJ, Ma H, Xu W, Lv R, Li X, Villen J, Gygi SP, et al. The histone H3 Lys 27 demethylase JMJD3 regulates gene expression by impacting transcriptional elongation. *Genes Dev.* 2012;26(12):1364-75.
46. Barski A, Cuddapah S, Cui K, Roh TY, Schones DE, Wang Z, Wei G, Chepelev I, and Zhao K. High-resolution profiling of histone methylations in the human genome. *Cell.* 2007;129(4):823-37.
47. Qi HH, Sarkissian M, Hu GQ, Wang Z, Bhattacharjee A, Gordon DB, Gonzales M, Lan F, Ongusaha PP, Huarte M, et al. Histone H4K20/H3K9 demethylase PHF8 regulates zebrafish brain and craniofacial development. *Nature.* 2010;466(7305):503-7.
48. Wang L, Feng Z, Wang X, Wang X, and Zhang X. DEGseq: an R package for identifying differentially expressed genes from RNA-seq data. *Bioinformatics.* 2010;26(1):136-8.

Figures and Figure legends

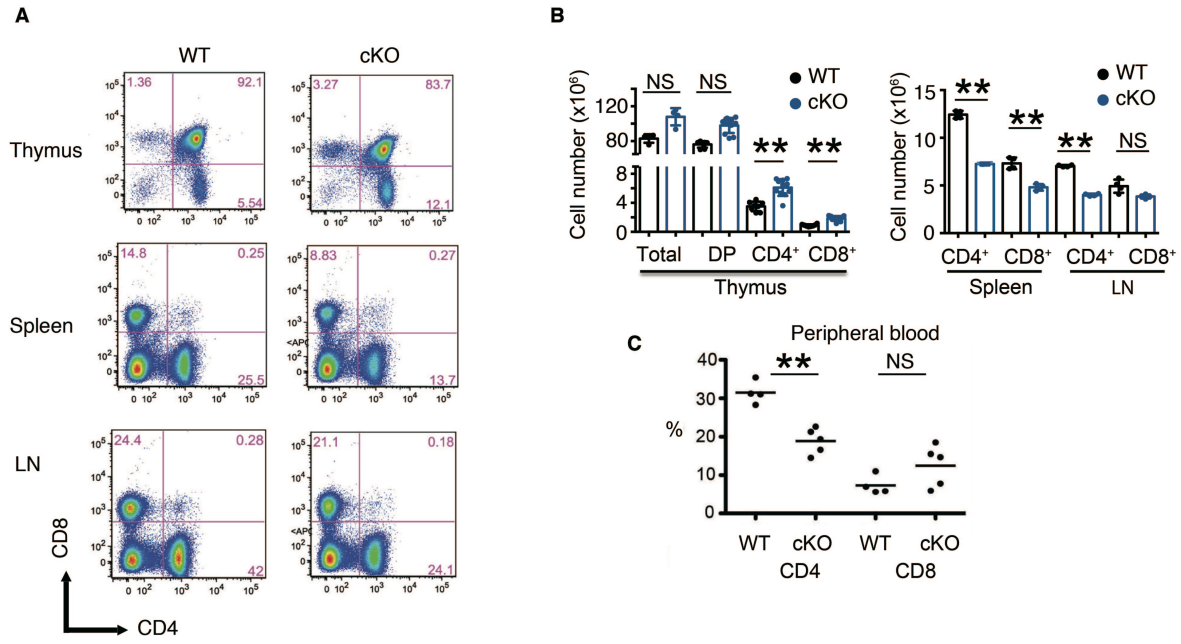

Figure 1. Analysis of T-cell populations in different organs of WT and *Jmjd3* cKO mice.

(A) Flow Cytometry analysis of CD4 and CD8 SP T cells in the thymus, spleen, and LN from WT and *Jmjd3* cKO mice. (B) Absolute cell numbers for different cell populations, including total, double positive (DP), CD4 SP, CD8 SP, $CD4^+$ and $CD8^+$ cells, in the thymus, spleens and LNs from WT and *Jmjd3* cKO mice (n=8/group, from 2 independent experiments). The data are reported as means ± SD from three independent experiments. Asterisks indicate significant differences between groups (**$P < 0.01$ determined by Student's t test). (C) Percentage of $CD4^+$ and $CD8^+$ cells in the peripheral blood from WT and *Jmjd3* cKO mice. Dots represent the individual mouse, and lines represent the mean. Asterisks indicate significant differences determined by Student's t test (n=4/5, **$P < 0.01$) (NS represents no significant differences).

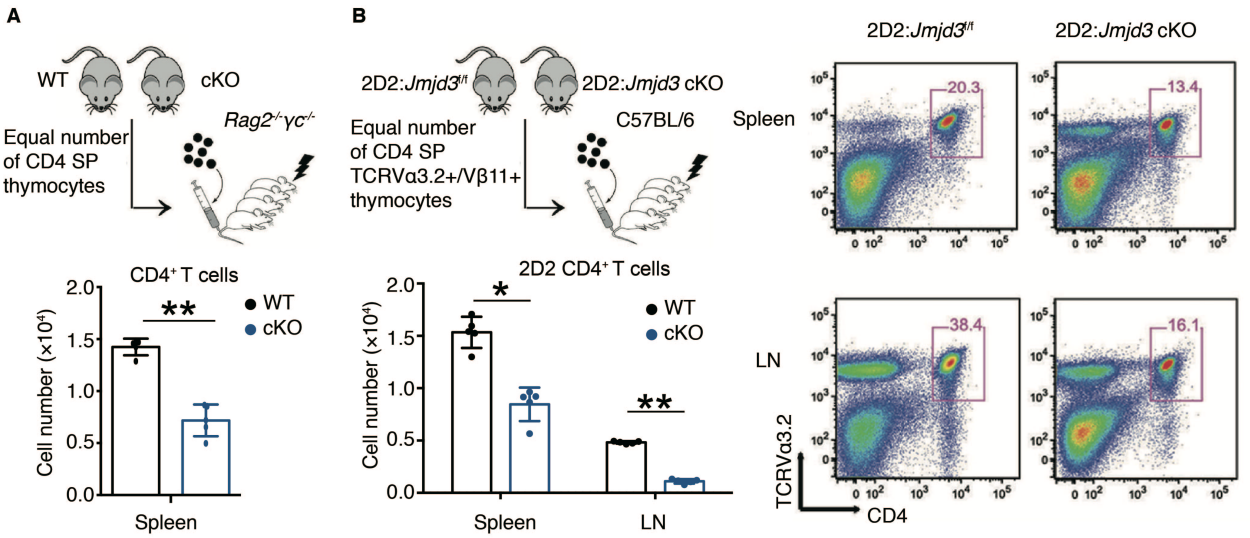

Figure 2. *Jmjd3* deficiency causes defects in T-cell migration.

(A) Thymic CD4 SP cells from either WT or *Jmjd3* cKO mice were purified by FACS, and equal numbers of cells were intravenously injected into sublethally irradiated *Rag2*$^{-/-}\gamma c^{-/-}$ mice (n=5) (upper panel). Absolute numbers of CD4$^+$ cells in the spleens of recipient *Rag2*$^{-/-}\gamma c^{-/-}$ mice were determined 24 h after adoptive transfer (lower panel). (B) Thymic CD4 SP (TCRVα3.2$^+$/Vβ11$^+$) T cells from either 2D2:*Jmjd3*$^{f/f}$ or 2D2:*Jmjd3* cKO mice were purified by FACS, and equal numbers of cells were intravenously injected into sublethally irradiated C57BL/6 mice (n=5). Absolute numbers of CD4$^+$ TCRVα3.2$^+$ TCRVβ11$^+$ cells in the spleens and LNs of recipient C57BL/6 mice were determined 24 h after adoptive transfer (left segment) and positive cells ratio (right segment) by FACS. The data are plotted as means ± SD from three independent experiments. Asterisks indicate significant differences between groups. *$P < 0.05$, **$P < 0.01$ determined by Student's t test

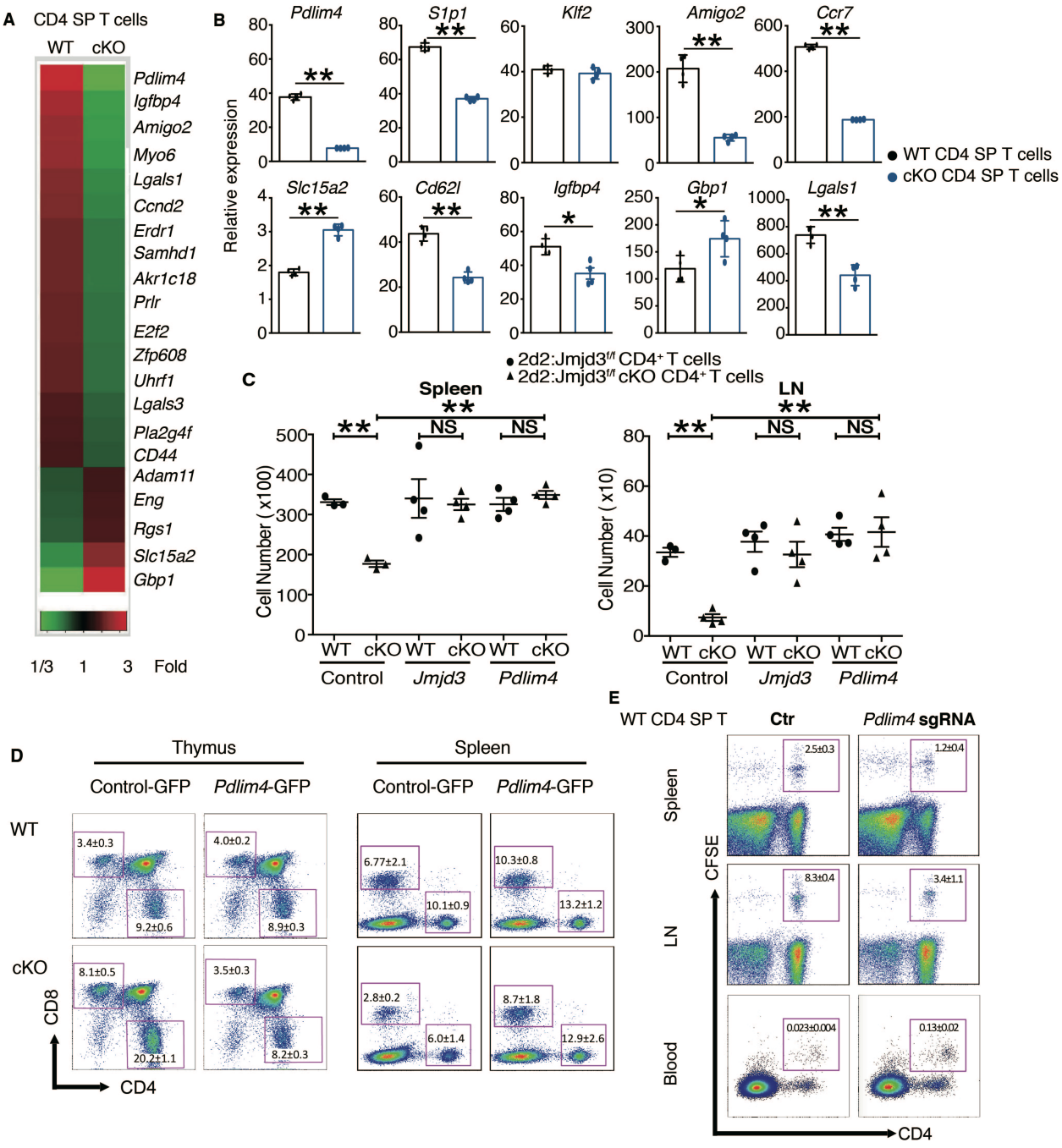

Figure 3. Identification of the JMJD3-target genes in CD4$^+$ T-cells and functional rescue of T cell defects by ectopic expression of Pdlim4.

(A) Heat map from microarray analysis of upregulated and downregulated genes in WT and *Jmjd3* cKO thymic CD4 SP T cells. (B) Real-time PCR analysis of a panel of genes between WT and *Jmjd3* cKO thymic CD4 SP T cells. Expression leves are given as the ratio of the target gene to the control gene to correct for variations in the starting amount of mRNA (gene/Gapdh x1000). (n=4, $*P < 0.05$, $**P < 0.01$ determined by Student's t test) (C) $CD4^+$ T cells from 2D2:*Jmjd3*$^{f/f}$ (WT) mice or 2D2:*Jmjd3* cKO mice were activated with MOG_{35-55} peptide in vitro before transduction with GFP-expressing retroviral vectors containing *Jmjd3* or *Pdlim4*. Equal numbers of GFP^+ $CD4^+$ T cells were intravenously injected into sublethally irradiated C57BL/6 mice (n=4). Absolute numbers of TCRVα3.2$^+$/Vβ11$^+$ GFP^+ $CD4^+$ T cells in spleens and LNs were determined by flow cytometry 48h after adoptive transfer. The data are presented as means ± SD from three independent experiments. Asterisks indicate significant differences between groups. $*P < 0.05$, $**P < 0.01$, by 1-way ANOVA with Tukey's multiple comparisons test. (D) WT and *Jmjd3*-cKO bone marrow cells overexpressing control-GFP or *Pdlim4*-GFP were transplanted into lethally irradiated C57BL/6 (WT) mice to generate chimeric mice. Flow cytometric analysis of $CD4^+$ and $CD8^+$ T cells from the thymus and the spleens of chimeric mice (n=3/group; 1 experiment). (E) Thymic CD4 SP T cells were isolated from WT mice. *Pdlim4* knockout was generated using the CRISPR-Cas9 system. Cells were labeled with carboxyfluorescein succinimidyl ester (CFSE), and then intravenously injected into sublethally irradiated C57BL/6 mice. After 48 hours, spleens, LNs, and peripheral blood were analyzed by flow cytometry for $CD4^+$ and CFSE-stained cells. The experiments were repeated three independent times (n=3/group; 1 experiment).

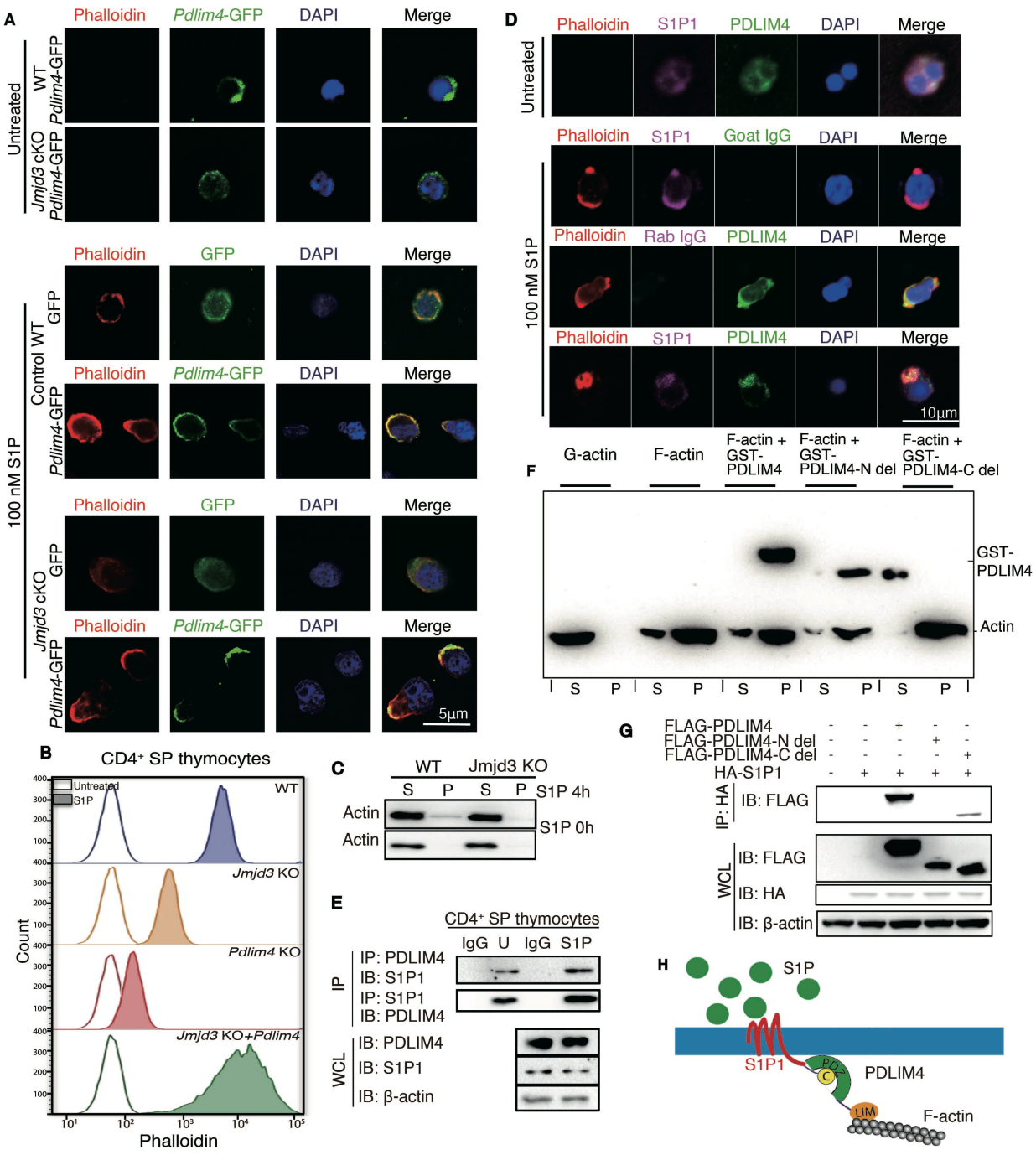
A
Phalloidin
Pdlim4-GFP
DAPI
Merge
Untreated
WT Pdlim4-GFP
Jmjd3 cKO Pdlim4-GFP
100 nM S1P
Phalloidin
GFP
DAPI
Merge
Control WT GFP
Pdlim4-GFP
Jmjd3 cKO GFP
Pdlim4-GFP
5μm
B
CD4+ SP thymocytes
Untreated
S1P
WT
Jmjd3 KO
Pdlim4 KO
Jmjd3 KO+Pdlim4
Count
Phalloidin
C
WT
Jmjd3 KO
S P S P
S1P 4h
S1P 0h
Actin
Actin
D
Phalloidin
S1P1
PDLIM4
DAPI
Merge
Untreated
Goat IgG
Rab IgG
100 nM S1P
10μm
E
CD4+ SP thymocytes
IgG U IgG S1P
IP
IP: PDLIM4
IB: S1P1
IP: S1P1
IB: PDLIM4
WCL
IB: PDLIM4
IB: S1P1
IB: β-actin
F
G-actin
F-actin
F-actin + GST-PDLIM4
F-actin + GST-PDLIM4-N del
F-actin + GST-PDLIM4-C del
GST-PDLIM4
Actin
S P S P S P S P S P
G
FLAG-PDLIM4
FLAG-PDLIM4-N del
FLAG-PDLIM4-C del
HA-S1P1
IP: HA
IB: FLAG
WCL
IB: FLAG
IB: HA
IB: β-actin
H
S1P
S1P1
PDZ
C
PDLIM4
LIM
F-actin

Figure 4. PDLIM4 regulates T-cell migration by interaction with S1P1 and modulation of F-actin reorganization

(A) Immunofluorescence microscopy images of WT and *Jmjd3* cKO CD4 T cells infected with lentivirus containing GFP or PDLIM4-GFP plasmids. Cells were starved 12 h and treated with 100 nM S1P for 3 h at 37°C. GFP or PDLIM4-GFP was detected with green fluorescence. Actin filaments were labeled with Rhodamine-conjugated phalloidin (red). Nuclei were stained with DAPI (blue). (B) FACS analysis of Phalloidin labeled F-actin in untreated and S1P treated WT, *Jmjd3* cKO, *Pdlim4* KO and *Pdlim4-expressing Jmjd3* cKO CD4 SP thymocytes. (C) The F-actin (pellet) and the G-actin (supernatant) from untreated and treated WT, *Jmjd3* cKO CD4 SP thymocytes were detected by Western blot. (D) Immunofluorescence microscopy of untreated and S1P treated WT $CD4^+$ SP cells stained with FITC-conjugated antibody to detect PDLIM4, Cy5-conjugated antibody to detect S1P1 and Rhodamine-conjugated phalloidin to detect actin filaments. Goat IgG and Rabbit IgG were used as isotype controls. Merged images indicate co-localization of proteins. (E) Co-IP analysis of endogenous interaction of PDLIM4 with S1P1 in untreated and S1P treated CD4 SP thymocytes. (F) Cosedimentation assay was performed using GST-PDLIM4, GST-PDLIM4 N-del, or GST-PDLIM4 C-del with F-actin, and subsequent analysis of supernatants (S) and pellets (P) by western blot analysis. (G) 293T cells were co-transfected with FLAG-*Pdlim4*-N-del, C-del, or full-length *Pdlim4* along with HA-*S1p1*. Whole cell lysates (WCLs) were immunoprecipitated with anti-HA beads and immunoblotted with anti-FLAG antibody. Three independent experiments were repeated with similar results. (H) A schematic diagram of the proposed model showing PDLIM4 interacts with the S1P1 protein at the N-terminal PDZ domain and binds F-actin by the C-terminal LIM domain.

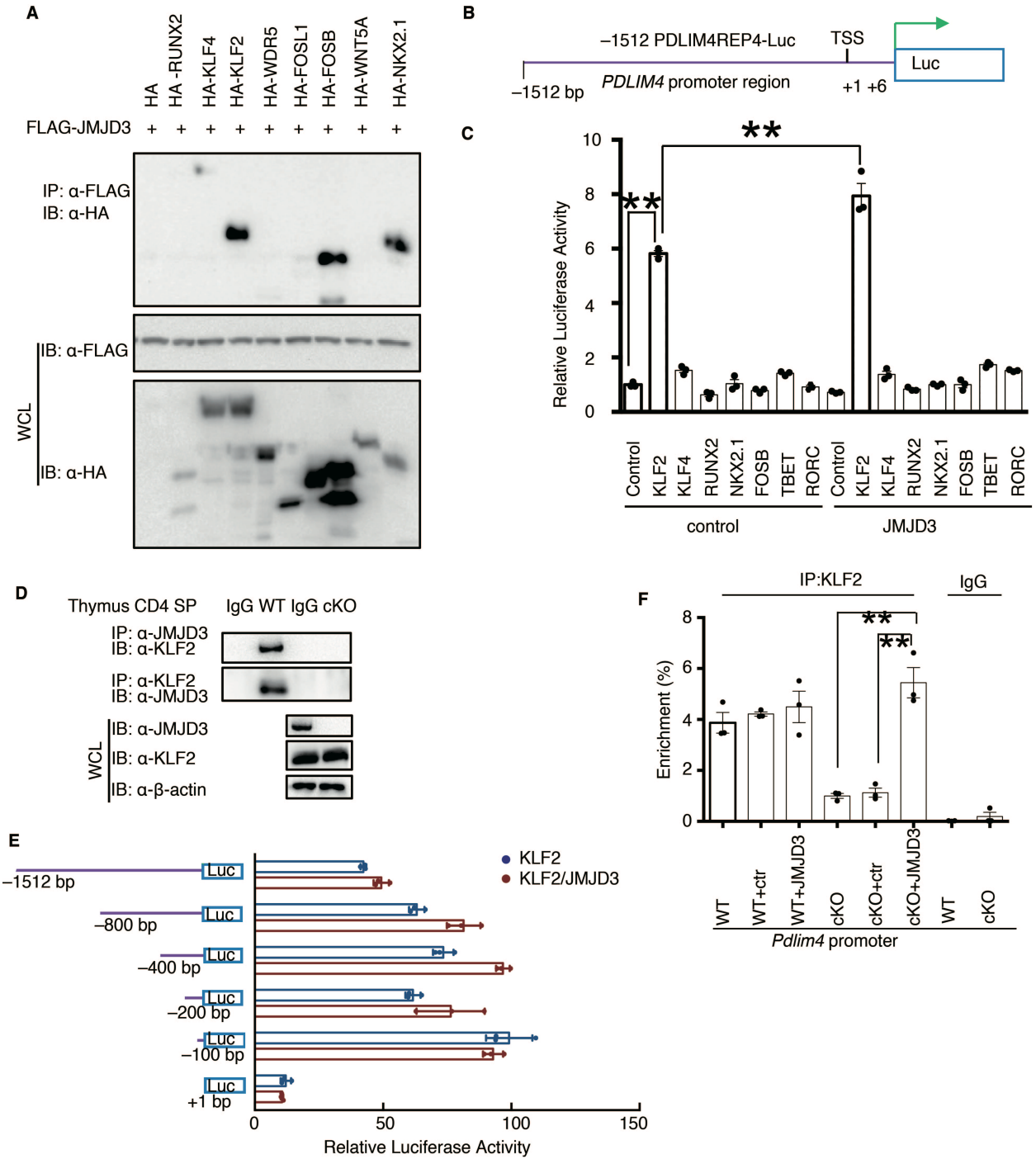

Figure 5. JMJD3 regulates *Pdlim4* expression by interacting with KLF2.

(A) Screening of transcription factors interacting with JMJD3. 293T cells were co-transfected with HA-tagged *Runx2*, *Klf4*, *Klf2*, *Wdr5*, *Fosl1*, *FosB*, *Wnt5a*, *Nkx2.1*, and FLAG-*Jmjd3*. Whole cell lysates (WCLs) were immunoprecipitated with anti-FLAG antibodies and immunoblotted with anti-HA antibody.

(B) Schematic presentation of the *Pdlim4* promoter-driven luciferase construct. The promoter region -1512 bp upstream was cloned into an episomal luciferase vector. (C) The transcriptional activity of proteins interacting with JMJD3 in regulating *Pdlim4* was evaluated by dual-luciferase assay. The data are presented as means ± SD from three independent experiments (n=3). Asterisks indicate significant differences between groups. $*P < 0.05$, $**P < 0.01$, by 1-way ANOVA with Tukey's multiple comparisons test. (D) Thymic CD4 SP T cells were isolated from WT and *Jmjd3* cKO mice and immunoprecipitated with anti-JMJD3 or anti-KLF2 antibodies and protein (A+G) beads. The immunoprecipitated product was immunoblotted with anti-KLF2 or anti-JMJD3 antibodies. (E) Mapping the KLF2 and JMJD3 binding regions of the *Pdlim4* promoter using a dual-luciferase assay. Different regions of the *Pdlim4* promoter were cloned into the episomal luciferase vector, and then were co-transfected with *Klf2* and *Jmjd3* into 293T cells. The data are presented as means ± SD from three independent experiments (n=3). Asterisks indicate significant differences between groups ($*P < 0.05$, determined by Student's t test). (F) ChIP-qPCR analysis of % enrichment of KLF2 at the *Pdlim4* promoter in WT and *Jmjd3* cKO thymic CD4 SP T cells after ectopic expression *Jmjd3*, IgG was used as isotype control. n=3, $*P < 0.05$, by 1-way ANOVA with Tukey's multiple comparisons test.

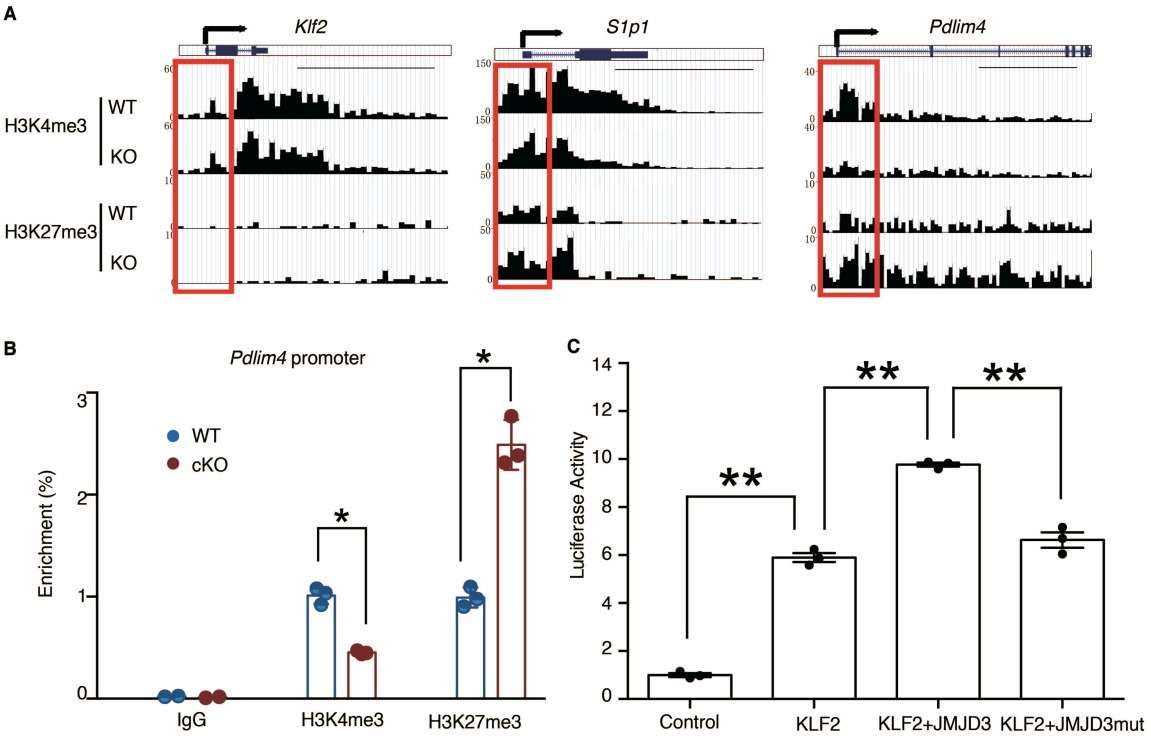

Figure 6. H3K27me3 and H3K4me3 levels in the *Pdlim4* promoter in WT and *Jmjd3*-deficient T cells.

(A) ChIP-Seq analysis of H3K27me3 and H3K4me3 levels in the promoter and gene body regions of *Klf2*, *S1p1*, and *Pdlim4* in thymic CD4 SP T cells isolated from WT and *Jmjd3* cKO mice. A 2-kb region around the TSS is indicated in a red box. Scale bars represent 5 kb regions. (B) Validation of methylation changes on the *Pdlim4* gene in WT and *Jmjd3* cKO CD4 SP T cells by ChIP-qPCR. The data represents mean ± SD from three independent experiments (n=3, **P* < 0.05 determined by Student's t test). (C) Luciferase assay was performed on 293T cells co-transfected with *Pdlim4* promoter-linked episomal luciferase vector and with *Klf2* in the presence of WT or mutant *Jmjd3* (a loss of demethylase function mutation). The data are presented as means ± SD from three independent experiments (n=3). Asterisks indicate significant differences between groups. **P* < 0.05, ***P* < 0.01 determined by 1-way ANOVA with Tukey's multiple comparisons test.

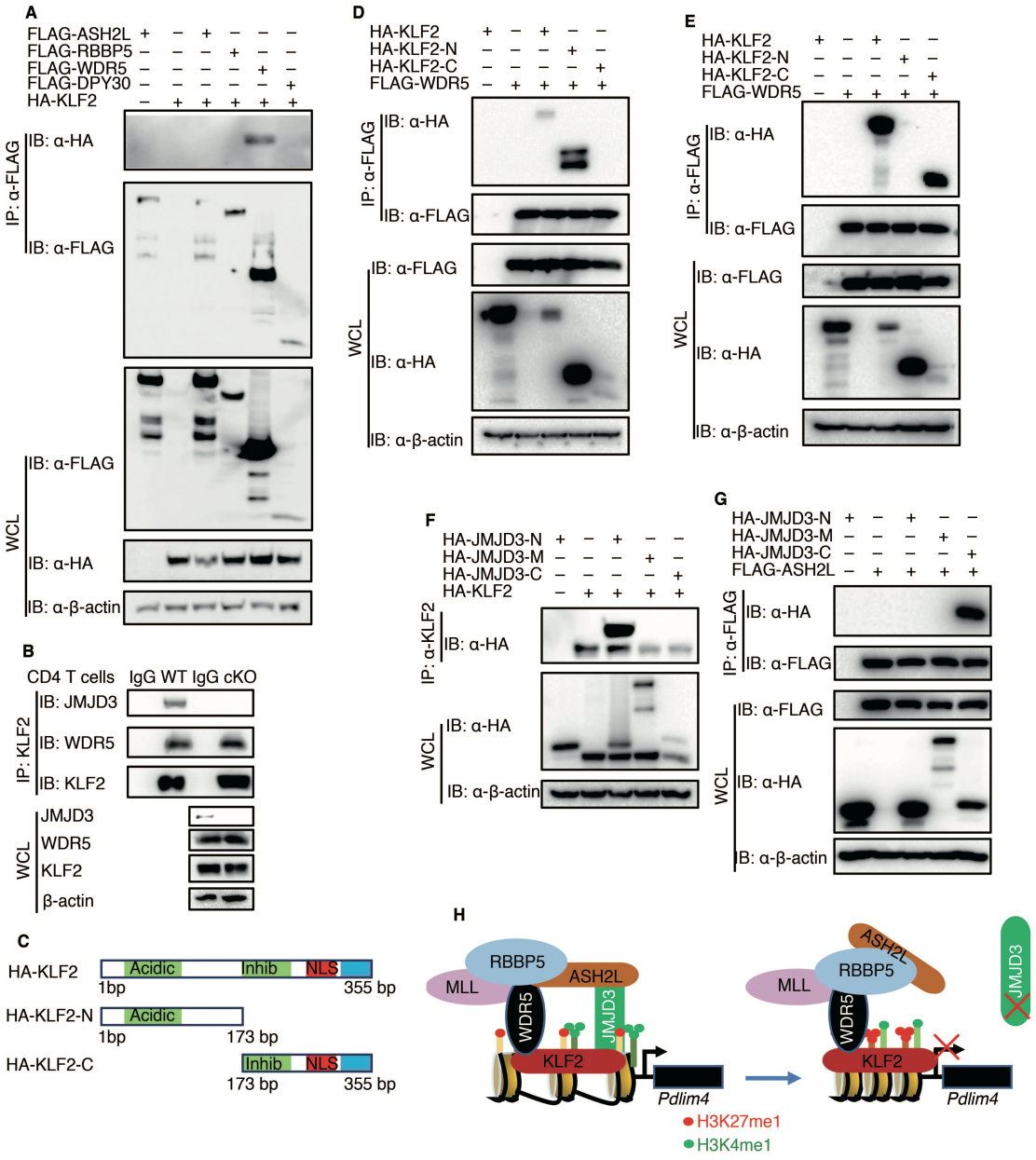

Figure 7. JMJD3 regulates PDLIM4 by facilitating the interaction between KLF2-WDR5.

(A) 293T cells were co-transfected with HA-*Klf2* and FLAG-tagged *Ash2L*, *RbBP5, Wdr5,* or *Dpy30*. Whole cell lysates (WCLs) were immunoprecipitated with anti-FLAG beads and immunoblotted with anti-HA antibody. (B) Cell lysates from WT and *Jmjd3* cKO CD4 SP T cells were immunoprecipitated with anti-KLF2 antibody and immunoblotted with anti-JMJD3, WDR5, and KLF2 antibodies,

respectively. (C) Schematic presentation of cloned HA-tagged N- and C-terminal regions of KLF2. (D) 293T cells were co-transfected with HA-N-terminal, C-terminal, or full-length *Klf2* along with FLAG-*Wdr5*. Whole cell lysates (WCLs) were immunoprecipitated with anti-FLAG beads and immunoblotted with anti-HA antibody. (E) 293T cells were co-transfected with HA-N-terminal, C-terminal, or full-length *Klf2* along with FLAG-*Jmjd3*. Whole cell lysates (WCLs) were immunoprecipitated with anti-FLAG beads and immunoblotted with anti-HA antibody. (F) 293T cells were co-transfected with HA-N-terminal, C-terminal, or middle region of *Jmjd3* along with HA-*Klf2*. Whole cell lysates (WCLs) were immunoprecipitated with anti-Klf2 antibody and immunoblotted with anti-HA antibody. (G) 293T cells were co-transfected with HA-N-terminal, C-terminal, or middle region of JMJD3 along with FLAG-*Ash2L*. Whole cell lysates (WCLs) were immunoprecipitated with anti-FLAG antibody and immunoblotted with anti-HA antibody. (H) Schematic diagram of proposed mechanism of how JMJD3 and KLF2 regulate *Pdlim4* expression. JMJD3 interacts with the MLL4 protein ASH2L and forms a stable complex with KLF2, which is capable of binding to the *Pdlim4* promoter. This permits JMJD3 to alter the H3K27 methylation state of *Pdlim4* and permits ASH2L to alter H3K4 methylation to control *Pdlim4* expression.